九州大学学術情報リポジトリ
Kyushu University Institutional Repository

Numerical Simulation of the Interference Effects to Outdoor Air Flow and Ventilation around Adjacent Building Arrays

Samuel Adinoyi Ayo
Department of Mechanical Engineering, Federal University of Technology Minna

Normah Mohd-Ghazali
School of Mechanical Enguneering, Faculty of Engineering, Universiti Teknologi Malaysia

https://doi.org/10.5109/7172303

出版情報：Evergreen. 11 (1), pp.402-416, 2024-03. 九州大学グリーンテクノロジー研究教育センター
バージョン：
権利関係：Creative Commons Attribution 4.0 International

Numerical Simulation of the Interference Effects to Outdoor Air Flow and Ventilation around Adjacent Building Arrays

Samuel Adinoyi Ayo[1,*], Normah Mohd-Ghazali[2]

[1]Department of Mechanical Engineering, Federal University of Technology Minna, Nigeria

[2]School of Mechanical Enguneering, Faculty of Engineering, Universiti Teknologi Malaysia, 81310 Johor Bahru, Johor, Malaysia

*Author to whom correspondence should be addressed:
E-mail: saayo1@gmail.com

(Received May 1, 2022; Revised March 10, 2024; Accepted March 18, 2024).

Abstract: The study examines the wind environment at the pedestrian level between two building arrays to determine the effect of the longitudinal separation distance (*W*) between the arrays of buildings for different height ratios (*HR*) of the arrays, on the outdoor air flow and ventilation, and provide a passive strategy of engendering higher wind motion and ventilation necessary for thermal comfort and human health. The study predicts the mean wind field around the arrays of buildings using the technique of numerical simulation. Results show that the ventilation performance strongly depends on the separation distance through the frontal and corner-stream inflows. The corner-stream flow was found to be able to account for about 50% of the total inflow. The optimum separation distances obtained for building configurations with *HR* = 1, *HR* = 1.5 and *HR* = 2, were respectively, *W*=12 m, *W*=30 m, and *W*=36 m. The increase in velocity ratio for these configurations ranges between 14% and 50%. The findings demonstrate that the separation distance between adjacent building arrays can be used to substantially increase the air motion and ventilation around building clusters and that corner-stream flow plays a very significant role in achieving the flow invigoration.

Keywords: air ventilation, air flow, building arrays, numerical simulation, separation distance

1. Introduction

The increasing urbanization in many developing and developed cities and the attendant need for more economic land utilization has caused buildings to be erected in clusters and in many cases with high-rise buildings located within the neighbourhood. This has precipitated the issue of inadequate air flow and ventilation in street canyons[1)], and the associated adverse effects on human health and thermal comfort both at the outdoor and indoor environments, since the quality of the air at the indoor space and the level of air motion are directly linked to those at the outdoor space[2,3)]. Air motion is one of the direct factors of human thermal comfort[4,5)]. It affects the rate of heat transfer by both convection and evaporation from the surface of human skin to the surroundings. On the other hand, air ventilation results in the exchange of heat and pollutant emissions arising from domestic anthropogenic sources such as urban environment vehicular and domestic activities with the cleaner upper atmosphere, mainly by advection and turbulence, to improve the air quality and enhance human health and thermal comfort[4,5)].

Developing strategies aimed at improving air flow and ventilation within and around buildings has been a major focus of several research studies. Zaki et al.[6)] studied cross-ventilation driven by wind in urban buildings using cubical building blocks for the effect of the position of window opening on the ventilation rate using numerical simulation employing the re-normalization group turbulence kinetic energy and the dissipation rate of the turbulence kinetic energy (RNG k-ε) turbulence model of the Reynolds-Averaged Navier–Stokes (RANS) model and reported best performance for the window position at the centre of the windward side and at the top of the leeward façade. In an earlier related study, Zaki et al.[7)] used wind tunnel experiment to examine the effect of urban air flow and dispersion on urban buildings wall pressure drag for different packing densities and ground surface roughness using different arrangements of arrays of rectangular blocks and established a relation between the bulk pressure coefficient and packing density as a rough measure for estimating wind-induced ventilation in urban buildings. Tan et al.[8)] used numerical simulation employing the RNG k- ε turbulence model and a Lagrangian model to examine the impact of air curtain mounted on ceiling on air flow and distribution of particles in a surgical zone and reported adverse effects of the use of the air curtain.

Methodologies for addressing urban air flow and ventilation problems can be broadly classified into two categories as passive and active. The more common, however, is the active strategy which essentially utilizes the mechanical air-conditioning system, mostly applicable for the indoor environment. The system relies heavily on the use of fossil deposits. But due to the increasing global demand for energy to support various aspect of human existence, the exhaustive nature and the hazardous impact of fossil fuels, efforts have continued to be made to device more efficient systems. Such research efforts include the study by Byrne et al.[9] in which the authors designed a solar system employing a phase change material storage system for powering a vapour-compression refrigeration air-conditioning system; the work by Kim et al.[10] optimizing the active indirect-type solar hot water systems at three different national locations; and a more recent study by Abirham et al.[11] in which they developed an ideal thermodynamic cycle for analyzing the performance of the adiabatic expansion-type solar thermal pumping system. These studies are, however, more suitable for addressing problems associated with indoor thermal comfort. Many studies dating back in time have therefore been directed at analyzing air flow and ventilation problems at the outside environment, particularly in street canyons[12 - 19].

Air flow and ventilation in street canyons around building arrays are strongly influenced by factors which include building packing density[12,13], building arrangement[14,15], and direction of ambient wind[16 – 19]. You et al.[15] used computational fluid dynamics (CFD) to simulate the correlation between various designs of residential building arrays and ventilation efficiency for different directions of wind flow and reported that wind direction was the most significant factor enhancing the wind environment around the building array, irrespective of the building arrangement design as determined by the geometric factors. Chen et al.[13] performed both CFD simulations and wind tunnel experiment to examine how the packing density of buildings affects the air flow and breathability of a city evaluated in terms of exchange velocity and velocity within the canopy for models of urban building arrays and reported that the normalized velocity within the canopy decreases significantly as the building packing density increases, unlike the normalized exchange velocity which changes only slightly. Buccolieri et al.[18] in their study to examine how the direction of wind flow affects the breathability of dense building arrays of different packing densities, reported that low wind angles result in minimal vertical and mean transversal pollutant transfers, with pollutant removal being due to longitudinal fluxes, while larger wind angles yield better ventilation arising from the increased vertical exchange and transversal fluxes. Yang et al.[14] examined, by numerical analysis, the impact of cross-ventilation across the upstream windows of a building on the flow field and pollutant distribution in street canyons and reported a decrease in pollutant concentration for window-opening-percentage ranging up to 10%, as a result of the in-canyon primary vortex being destroyed. However, the study was for isolated street canyon of uniform building heights.

Apart from the thermal comfort and health benefit of enhanced flow and ventilation for people outdoors, the need for the indoor occupants has also been highlighted[20]. The studies have therefore not been limited to only the outdoor environment but the influence on the indoor environment has also been examined. Mohammed et al.[3] performed wind tunnel experiment using cubical block arrays to study the impact of outdoor urban canopy flow on indoor air flow for different positions of the array openings and reported that the indoor and outdoor airflows are correlated. They further reported that the inflow is due primarily to the turbulence induced by the surrounding buildings at the outdoor and that the positions of the array openings significantly affect the indoor space mean wind speed. It is, thus, evident that there has been active interest in the study of air flow and ventilation in the urban environment to address the adverse impact of urbanization on the thermal comfort parameters. Wulandari et al.[21] used computer simulation to examine how layout arrangement could be used to improve the cooling of an Information technology (IT) rack of a data centre room and reported that there was improvement in the cooling when the rack was arranged in accordance with the American Society of Heating, Refrigerating and Air-Conditioning Engineers (ASHRAE) recommendations. Yinn et al.[22] also demonstrated the importance of enhanced air motion for an indoor environment in their study in which they examined the influence of turning motion of medical personnel on the air flow distribution in a surgical room.

From the foregoing, it would be observed that in most of the previous studies, particularly those on the outdoor environment, attention has mostly been focused on determining and comparing values of air flow and ventilation parameters for different climatic characteristics and building configurations. No significant attempt has been made to examine the mechanism of flow of some of the features and taking advantage of it in deploying it to enhance air ventilation. In the present work, it is thought that if proper understanding of the mechanism of flow around building arrays in adjacent locations is taken advantage of, especially as it concerns corner-stream flow[23], it becomes much easier for interactive adjacent building clusters to be laid out in such a way that enhances air flow and breathability. The main focus of this study is, thus, to examine the mechanism of air flow and ventilation around arrays of buildings in adjacent locations, in which one of the arrays has a significant adverse influence on the air flow and ventilation around the other array. The objective is to utilize the knowledge of the mechanism of flow to determine the influence of the separation distance of the building arrays on the air flow and ventilation at the pedestrian level of the streets, for

various ratios of heights between buildings and identify the configurations that would ensure optimum values of relevant ventilation parameters necessary for human thermal comfort. The outcome is expected to be of benefit to developers in the building industry and government urban renewal agencies in the proper layout of buildings in complex clusters and partly address natural airflow and ventilation problems that are often associated with high-rise buildings erected at the upstream location, within the neighbourhood of buildings of lower height, especially in low-wind and humid climates.

2. Methodology of the research

2.1 Physical modelling and configuration of the building layout

The study is set in a sub-urban neighbourhood of Kuala Lumpur, Malaysia. Malaysia has generally been identified as a low-wind, hot and humid country, with available data describing the mean wind speed as below the level recommended for thermal comfort, unsuitable for driving natural ventilation at the indoor space[24]. For example, Hanipa et al.[25] put the mean wind speed around the capital city of Kuala Lumpur to range from 1.63 m/s to 1.7 m/s; Wen et al.[26] stated the mean velocity in Malaysia to be between 2 m/s and 3 m/s; and Ayo et al.[27] reported the mean wind speed around Kuala Lumpur as 1.52 m/s. Observed that these wind speeds are normally measured around open terrains far from the built-up areas and at 10 m meteorological height above the ground level[26] which would be much lower at the pedestrian-level height of between 1.5 m and 2 m, the mean wind speed in Malaysia, particularly around the Capital City of Kuala Lumpur, is below that necessary for thermal comfort at the indoor space suggested to range between 0.1 m/s and 1.5 m/s[28]. Given the draw-backs of mechanical air-conditioning system application earlier outlined, it is necessary to explore the passive strategy of using appropriate layout of buildings to improve air flow and ventilation around clusters of buildings around many of the cities, including the Capital City.

By By-Law 42 of the Malaysia Uniform By-Laws (UBBL) 1984, which stipulated the minimum area for a habitable room to be 6.5 – 11 m^2, with a minimum width of 2 m for a residential building[29] and taking into consideration the interference effect which increases with the lateral dimension of a building, a building plan with depth 10 and width 40 m was adopted for the study. In the study by Yim et al.[1], it was shown that a single column of high-rise upwind buildings creates an interference effect to a three column lower-rise buildings at the downwind location. Also, by Malaysia Planning Guideline (GP022)[30], low-rise building classification is designated for a building of a maximum of four storeys, which the authors of the present research have observed to be quite prevalent in most cities of the Country, including Subang and Johor. In this study therefore, the meteorological conditions of the Capital City and a cluster of four-storey buildings subjected to the interference effects of a taller building array at the upwind location are referenced. The study, thus, employs actual meteorological data collected from the nearby Subang Meteorological Station which were processed into their mean values and the associated turbulence quantities and utilized as input. A 1 x 3 array of buildings at the upwind location and a 3 x 3 array downwind, all in in-line arrangement, were used to represent the adjacent building arrays. Each of the downwind buildings has the building envelop dimensions as 40 m width (W), 12 m height (H), and 10 m depth (D). The upwind buildings have similar dimensions of the width and depth, but the heights vary from 12 m to 30 m by 6 m step. As mentioned previously, the room units are dimensioned following the Bye-Law 42 of Malaysia.

The impact of the separation distance on the air flow and ventilation around the downwind building array is examined by considering thirty configurations of the arrays produced by increasing the separation distance (W) between the 1 x 3 frontal array and the downwind 3 x 3 array, in the longitudinal direction from 12 m, which is the height (H) of the downwind building array, to 36 m = 3H, by 6 m = ½H. The upwind building height is varied from 12 m to 36 m also by the same step increase of 6 m. The longitudinal separation distance (W_c) of the 3 x 3 array was fixed at 18 m based on a survey by the present authors which revealed the prevalence of the value of the separation distance around arrays of low-rise buildings around the reference study area. The lateral passage between the buildings has a constant width w = 6 m, following Guidelines (GP022) of Malaysia. The geometries and layouts of the two arrays of buildings are as depicted in Figs. 1 and 2, respectively.

2.2 The study approach and numerical simulation

In this study, the flow around the building arrays is assumed to be turbulent. A numerical solution procedure which utilizes the computational fluid dynamics (CFD) technique is, thus, employed in solving the governing conservation equations for the flow fields. The technique uses the Realizable turbulence kinetic energy (RKE) turbulence model[31] to predict the fields of flow around the full-scale size of the building arrays. The model has been used extensively in previous research studies to examine boundary layer flows and wind flow around buildings and reported to perform quite well[32,33]. The model has also been observed to outperform other RANs models like Standard turbulence kinetic energy (SKE) and Re-Normalized Group turbulence kinetic energy (RNG KE) for flow situation that includes separated flows as characterise the recirculation flows that are expected to prominently feature in the present study case. In comparison, Large Eddy Simulation (LES), because it explicitly calculates many scales of turbulence and models small portions of Reynolds stress and scalar fluxes that are much smaller than those in RANS models, entails higher

simulation complexity and, thus, demands large computational resource[34]. As a result, there appears to be a preference for Realizable turbulence kinetic energy model when simulation turbulent flow problems, particularly, atmospheric boundary layer flows and flows around buildings[32,33].

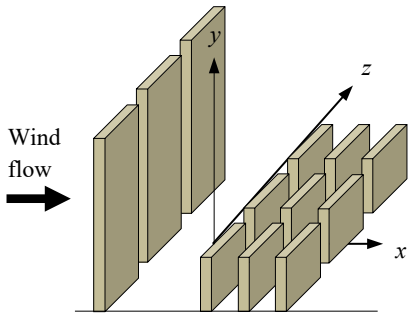

Fig. 1: Layout of the adjacent building arrays

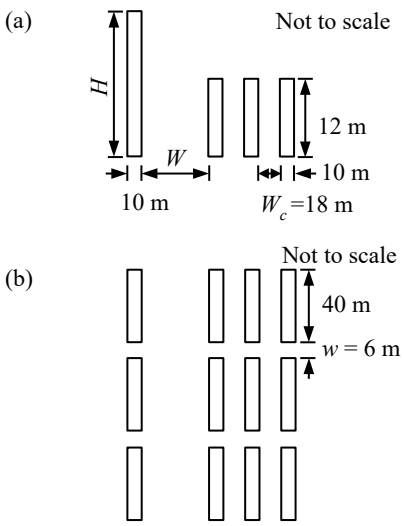

Fig. 2: Geometries and layout of the arrays, (a) Side view, (b) Top view

In an urban boundary layer, the flow can be modelled by the conservation laws of fluid flow. Following Hoydysh[35], the regime of flow is turbulent if the Reynold's number $Re_H \geq 3400$, where $Re_H (= UH/\vartheta)$ indicates that the Reynold's number is based on the building height H; U being the wind speed at H and ϑ the kinematic viscosity of the air. In the present study, Re_H was evaluated as $Re_H = 690000$, using the height of the downwind low-rise building cluster as reference. This confirms the turbulent flow regime assumption made earlier.

The computational domain for the flow field calculation was designed following the recommendations of past studies and major guidelines[36,37]. The conditions at the boundaries for the velocity vector $\boldsymbol{V}$, the turbulence kinetic energy k, and the rate of dissipation of the kinetic energy ε, the gradients of the variables and that of pressure were specified appropriately. At the inflow boundary, the vertical profile of velocity was based on the ten-year (2003 – 2012) wind data obtained from Subang Meteorological Station. The mean wind speed of 1.52 m/s at the meteorological height of 10 m was adjusted appropriately for the urban location of the study area to yield 0.92 m/s as the applicable mean wind speed at the study site. The profiles at the inflow for the horizontal velocity U, the k and ε were specified in accordance with the guidelines of the European Cooperative in the Field of Scientific and Technical Research (COST) employing the relations suggested by Richards and Hoxey[38]. Conditions at the two lateral and top boundaries were prescribed by the inviscid wall boundary condition. At the outflow boundary, the variables were specified by the exit boundary conditions. The boundary condition assumes that at the exit the flow has become fully developed, as such the gradients of all flow parameters are zero. At the solid boundaries of the building walls surfaces, conditions were specified by wall-functions following Tominaga et al.[37] to prescribe the U, k and ε conditions at the cells adjacent to the walls as follows:

$$\frac{U_p}{u^*} = \frac{1}{\kappa} ln\left(\frac{u^* y_p}{\nu}\right) + B \qquad (1a)$$

$$k_p = \frac{u^{*2}}{\sqrt{C_\mu}} \qquad (1b)$$

$$\varepsilon_p = \frac{u^{*3}}{\kappa y_p} \qquad (1c)$$

where U_p, k_p, ε_p are the tangential component of the horizontal wind velocity U, the k and ε, respectively, at point P which is the mid-point of the wall-adjacent cells, and y_p is the distance from point P to the wall. $u^* = C_\mu^{1/4} k_p^{1/2}$, B is a universal constant, C_μ is a Standard k-ε model constant and k is the von Karman constant. B, C_μ, and k have values as follows: $B \approx$ 5-5.5, $C_\mu = 0.09$, and $k \approx$ 0.4-0.42. The constants are as prescribed in the relations suggested by Richards and Hoxey[38] for computing the values of U, k and ε at the wall-adjacent cells.

The mean velocity condition for the rough ground surface at the wall-adjacent cells was specified by the wall-function expressed as[39],

$$\frac{U_p}{u^*} = \frac{1}{\kappa} ln\left(\frac{u^* y_p}{\nu C_S K_S^+}\right) + 5.43 \qquad (2)$$

where K_S^+ is the dimensionless surface roughness height, K_S is the dimensional roughness height, and C_S is surface roughness constant and has value in the interval 0, 1.

The computational domain was discretized using the unstructured tetrahedral mesh elements. Compared to hexahedral mesh, tetrahedral mesh has been observed to be more closely adaptive to a flow domain having a complicated boundary[40] such as characterizes the irregular ground surface in the present research, and

adequately capture the details of the flow situation in the regions close to the surface. Finer mesh elements were concentrated around the ground and building surfaces, and building corners. At the regions far from the solid surfaces, larger mesh elements were used, having gradually increased from their fine sizes at the solid surfaces by expansion ratios not more than 1.2. The elements have aspect ratios ranging between 0.5 and 20[39]. The roughness parameter y_0 for a sub-urban residential area is 0.5 m[1]. However, due to the need to locate the pedestrian-level evaluation height at the third or higher grid from the ground surface[41,38] a smaller value, y_0 = 0.02 m, was selected.

Grid sensitivity test was performed to ensure the simulation results were had become independent of the number of meshes. The test was conducted for each of the configurations simulated by initially employing a default no of meshes and then continually refining the meshes and comparing results of the current simulation to that of the preceding one, until the difference in results of the average wind velocities at the pedestrian level height for the last two consecutive grids is less than 5%, following Buccolieri et al.[12]. The meshing with the lower number of grids was then chosen for the simulation. The number of the grids eventually used in the simulations ranged from 2.5 million for the configuration with the smallest domain size, with *HR* = 1, *W* = 12 m, to 5.5 million for the one with the largest domain size, with *HR* = 3.0, *W* = 36 m.

The model equations were then computed using the pressure-based solver. The algorithm based on the Semi-Implicit Method for Pressure-Linked Equations (SIMPLE) was adopted for solving the pressure-velocity coupled equations. Compared to other algorithms such as the revised form of SIMPLE, called the Semi-Implicit Method for Pressure-Linked Equations-Revised (SIMPLER) which tends to have better performance in many flow cases owing largely to the lower number of under-relaxation factors required, on per iteration basis the SIMPLE algorithm is known to be cheaper. As a result, for turbulent flows, as is the case in the present study, when optimal combination of under-relaxation factors is utilized, the SIMPLE algorithm has been found to perform better[42]. The algorithm has been used extensively in previous studies[27,43].

The inflow boundary conditions were implemented in the solver by coding the profiles for the mean wind speed, k and ε in user-defined functions (*udf*). To implement the lateral and top boundary conditions of the computational domain, the zero shear conditions at the surface were specified in the solver, while the outflow boundary condition were specified to implement conditions at the exit boundary. For the wall-adjacent cells of the surface of the ground, the mean velocity was calculated by implementing equation (2). The values for k and ε at the cells are specified by implementing equation (1). To achieve this, the ground terrain roughness height was specified as $y_0 = 0.02\ m$, corresponding to a grass land terrain having grass cover in the range between short and long grass[44], while the roughness constant, $C_S = 1.0$. For the building surfaces, the wall-functions for a smooth surface as expressed by equations (1) are implemented, with the roughness height specified as zero in the solver.

The iteration process of the computation was controlled for convergence by specifying a scaled residual of $1\text{x}10^{-5}$ that was uniform for all the variables. The computation of governing model equations was carried out at the Centre for Information and Communication Technology (CICT) Unit of Universiti Teknologi Malaysia (UTM), Malaysia using the Centre's high-performance computer (HPC) system.

The simulation yields the mean velocity flow field, consisting of the *x*-, *y*-, and *z*-mean velocity components. Together, they form the data for evaluating the air flow and ventilation performance characteristics of the different configurations. There was a total of 30 configurations, ranging from the smallest with *W*=12 m, *HR*=1 to the largest with *W*=36 m, *HR*=3. Several runs of the simulations that were at least two and a half times the number of configurations were carried out, both trial and final runs. The run-time for the smallest configuration with about 2.5 million cells was between 45 minutes and 1 hour. The larger configurations took between 3 and 5 hours.

2.3 Air ventilation performance indicators

The magnitude of air flow around the building arrays was assessed by a criterion called air velocity ratio (*VR*), while the level of air ventilation of the arrays was measured in terms of air flow rate (*AFR*). The air velocity ratio is a dimensionless quantity defined as the ratio of the mean wind speed at the pedestrian level, usually at a height 2 m above the ground level, to the wind speed at the boundary layer height[45]. The air flow rate is a measure of the ability of the building array at the downwind location to exchange the domain air with that of the surrounding environment[12]. The air flow rate is non-dimensionalised with the air flow rate at an upwind location at which the presence of the buildings does not have an effect, and can be expressed as

$$AFR = \frac{q}{q_{ref}} = \frac{\int_A \vec{V}.\vec{n}dA}{\int_A \vec{U}_{ref}.\vec{n}dA} \qquad (3)$$

where q and q_{ref} are the rates of air flow through the openings of the objective domain and that across an equivalent area at a reference location far upwind, respectively; $\vec{V}$ and $\vec{n}$ are the velocity vector and the unit vector orienting the openings, respectively; and A is the area of the opening. $\vec{U}_{ref}$ is the velocity vector in the streamwise direction, at a location far upwind of the array of buildings, through an opening with area equivalent to that of the frontal opening. Equation 3 was used to calculate the rate of air flow across the external openings of the array of buildings.

In determining the *AFR* for a target region, mass flow

balance was applied across the external openings of the volume in order to estimate the total amount of air flow rate across all boundaries of the control volume. For the adjacent building arrays configurations employed in this study, the measurement planes used to determine the *VR* are shown in Fig.3, while the domain of the downstream array of buildings used as the control volume to determine *AFR*, and the openings of the domain are as shown in Fig. 4.

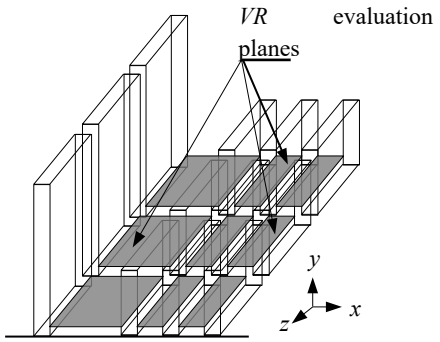

Fig. 3: Planes for evaluation of *VR* for the building arrays

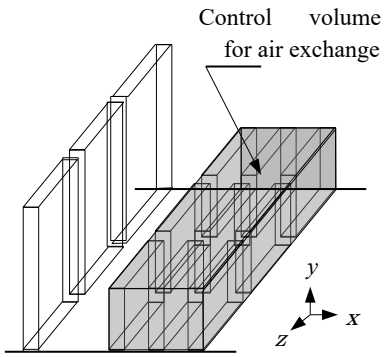

Fig. 4: Geometries for evaluating *AFR* for the objective building array

2.4 Validation of the turbulence model

The validation was conducted to ascertain the capability of the model to predict satisfactorily the field of flow around the arrays of buildings. The validation compares the RKE turbulence model prediction of the flow of air around scaled models of city blocks with data from wind tunnel experiment performed on the city blocks at the (Japanese) National Institute for Environmental Studies[46]. These data have been used extensively for similar validation purposes in previous studies[47]. The layout of the model city blocks and the measurement geometries are shown in Fig. 5[46], with Fig.5(a) being the side view, while Fig.5(b) is the plan.

The computational domain for the validation process was designed following similar procedure as was to be employed for the actual array of buildings under study, the details of which are shown in section 2.2. The boundary conditions for the computational domain were specified from the data obtained from the experiment. The data for the inflow profile which were provided in graphical form were carefully extracted and fitted with appropriate curves to yield the mean wind speed profile at the inflow boundary. The velocity variances and the inflow turbulence kinetic energy were determined using the roughness length, the roughness Reynolds number, the friction velocity and the scaled velocity variances provided from the experiment. The profile of the dissipation rate of turbulence kinetic energy of the approach flow was calculated using the expression by Richards and Hoxey[38]. Other boundary conditions, such as the wall-function for U, k, and ε at the wall-adjacent cells of the solid building boundary surface and floor of wind tunnel were implemented as done for the actual building arrays, the details of which are shown in section 2.2. The results of the validation of the CFD turbulence model are presented in section 3.

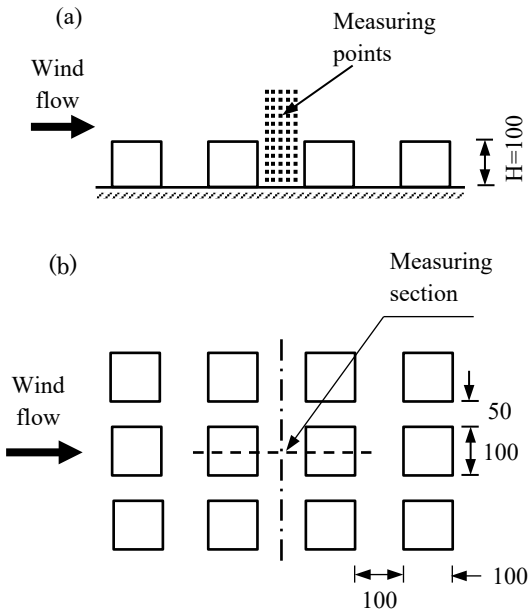

Fig. 5: Experimental models setting and the points of measurement (in mm)

3. Results

3.1 The CFD simulation validation results

In order to validate the CFD model, it was first ensured that the input profile of the approach flow wind velocity at the inflow boundary is appropriately specified for the simulation. This was done by comparing the actual profile of the wind tunnel experimental data with the approximate function of the data profile employed for the validation of the CFD simulation. The result of the comparison is shown in Fig. 6. The result demonstrates that the approximating function follows closely the profile of the data of the measured wind speed, giving the authors the confidence that values of the experimental data were correctly specified. The result of the CFD validation is shown in Fig. 7.

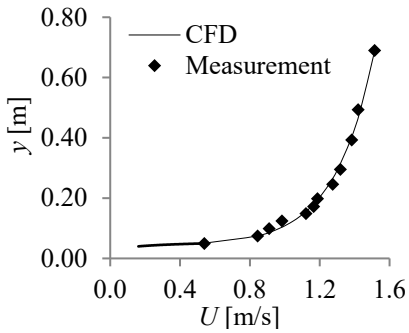

Fig. 6: Comparison of profile of measured vertical wind velocity of approach flow with that of the CFD approximation

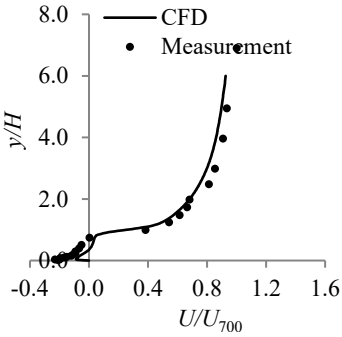

Fig. 7: Comparison of profile of measured normalized streamwise velocity with the calculated profile at centre of target street

The figure compares the profile of the measured streamwise velocities at the centre of the target street with the profile of the calculated velocities at corresponding points of the street location in the simulation. The profile of the velocity in the streamwise direction U was normalized with the free stream velocity U_{700} at a height 700 mm from the ground floor. It is shown in the figure that at the street centre, the pattern of the results of the simulation is similar to that of the experimental data. It could also be seen from the figure that the simulation result closely follows that of the experimental data, particularly in the region $y/H \geq 1.0$, the higher wind region. It is further indicated in Fig. 6 that the turbulence model is able to reproduce the the re-circulation vortex located within the street canyon as present in the experiment. However, in the weak wind region, particularly for $y/H < 1.0$, the mean wind speed was calculated a little lower than the experimentally measured values. The centre of the recirculation vortex is also slightly calculated lower than that produced in the wind tunnel experiment. These results are consistent with those of Yoshie et al.[48] and Yim et al.[1]. The visual agreements observed from the measured and calculated normalized streamwise velocities in Fig. 7 are quantified to further establish the strength of the turbulence model in predicting the field of flow around the arrays of buildings following the procedure by Ayo et al.[27] and Jenssen et al.[33] and presented as shown in Fig. 8.

On the graph in Fig. 8, the experimental values of the scalar normalized streamwise velocities at each of the measurement points and their corresponding calculated values are plotted with equal scales on the horizontal and vertical axes, with the data series formatted using a marker shape. A second plot of a line representing zero deviation or 100% agreement (indicated 0% on the graph) between the measured and calculated values is plotted, which would appear as a diagonal of the graph. Two other lines, one on each side of the diagonal, which would capture the majority of the actual data series of the measured and calculated velocity values are plotted and the degree of deviation of the lines on both sides of the diagonal, which represent the accuracy of the calculated velocity values, are determined. Two sets of such lines, indicated as ±10% and ±15%, are plotted in Fig. 8.

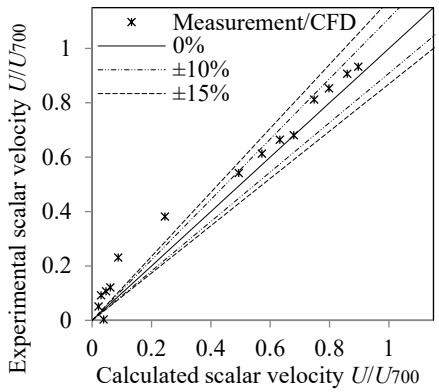

Fig. 8: Quantification of the accuracy of the calculated profile of normalized streamwise velocities at centre of target street

From Fig. 8, it would be seen that the majority of the calculated data series of the numerical simulation lie within the 15% deviation from the measured data series, particularly at higher altitudes at which the wind velocities are higher. At the lower wind regions close to the ground floor, the wind velocities are predicted a little bit lower, with very few outliers observed. Following Cheung and Liu[49], the 15% error margin obtained from this analysis is considered acceptable in engineering tolerance.

When compared to the results of previous validation[47] conducted for when the condition of the atmosphere is unstable, the results obtained in the present study shows a better performance of the numerical simulation. This may be attributed to the configuration adopted for the present validation which was 3-D, a more realistic configuration, compared to the assumed 2-D configuration employed in these previous studies. It may also be due to the isolated street canyon configuration employed in the studies instead of a street canyon within an array of buildings. Besides, the closely approximating inflow horizontal approach flow velocity profile employed at the inlet boundary of the computational domain instead of the

uniform vertical profile prescribed in the previous studies might have also accounted for the better performance achieved in the present study. Considering the overall satisfactory performance of the turbulence model, it was believed that the model is sufficiently robust in predicting a realistic wind field around the adjacent building arrays under investigation. The investigation of the different configurations of the arrays of buildings for the air ventilation performance was, thus, proceeded with to be carried out by the turbulence model.

3.2 Air ventilation performance results of the adjacent building arrays

Results of performance of the adjacent arrays of buildings for the air ventilation characteristics measured in terms of *VR* and *AFR* are presented., The results are given for the different sections of the streets. For reference purpose, the street sections are designated as shown in Fig. 9. Due to symmetry of flow around the arrays of buildings, the half-domain configuration of the building arrays was employed. The lateral street separating the frontal building array from the one at the rear is termed "Separation Street or SS". The section of the street towards the middle of the arrays is designated "Separation Street Middle or SSM", while that towards the side is "Separation Street Edge or SSE". Each of the lateral streets of the rear building array is designated "Main Street or MS", with the one at the upwind location termed "Main Street 1 or MS1", while that downwind is "Main Street 2 or MS2". The main streets (MS1 and MS2) are each segmented into "Main Street 1 Middle or MS1M" and "Main Street 1 Edge or MS1E" for MS1 and "Main Street 2 Middle or MS2M" and "Main Street 2 Edge or MS2E" for MS2 to indicate, respectively, those street sections towards the middle of the building arrays and those towards the edge. The narrow street that runs along the longitudinal axis (streamwise direction) of the building arrays is termed "Secondary Street".

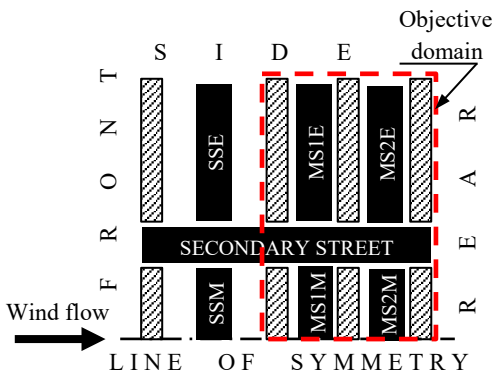

Fig. 9: Streets designations for half-domain of the building arrays in top view

Figs. 10(a) – (f) show the velocity ratio profiles for all the street sections: SSE (Fig.10(a)), SSM (Fig.10(b)), MS1E (Fig.10(c)), MS1M (Fig.10(d)), MS2E (Fig.10(e)), and MS2M (Fig.10(f)) of the downwind building array at the pedestrian level height, while Fig.11 shows the characteristics of the air flow rate around the array, as the *AFR* is dependent on the separation distance between the building arrays, for various height ratios. From Figs. 10(a) – (f), it would be seen that the velocity ratios vary with height ratios as well as the separation distances except for *HR* = 0, the case of the low-height building standing in isolation, without any other building array present at the upwind location.

From the figures, it could be observed that the presence of the upwind buildings represented by *HR* = 1.0 to *HR* = 3.0 causes a reduction in the air velocity ratio in the streets of the downwind building array, in comparison to the case when there is no building upstream. At MS1E, the reduction may be as much as from *VR* = 0.2054 to *VR* = 0.0389, representing about 81%, at MS2E from *VR* = 0.1635 to *VR* = 0.0509, representing about 69%, at MS1M from *VR* = 0.1602 to *VR* = 0.0629, representing about 61%, and at MS2M from *VR* = 0.1036 to *VR* = 0.0626, representing about 40%. A careful inspection of Fig.10(c) to Fig.10(f) would indicate an interplay of flow entering the building arrays through the frontal openings, and the corner-stream[50,51] inflow through the lateral openings. It would mean that at small height ratios the quantity of flow of the incoming approach flow to the windward building face which is deflected as corner-stream and the length of throw of the stream at the leeward side is small, and at higher height ratio, the quantity of the flow and the length of throw is greater.

At low height ratios and small separation distances, e.g., $1.0 \leq HR < 2.0$, $12\text{ m} \leq W < 24\text{ m}$ observed in Figs. 10(c) and (e) therefore, the tendency is for the street flow at MS1E (Fig. 10(c)) to be equally minimally influenced by the frontal and corner-stream inflows, producing a *VR* of between 0.08 and 0.1275, but at MS2E (Fig. 10(e)) the flow appears to be influenced more by the corner-stream as more of the flow is intercepted into the street and the reach of the frontal inflow is reduced. The higher quantity of corner stream inflow may therefore account for the higher *VR* of between 0.1354 and 0.2325 observed in Fig. 10(e). As the separation distance increases, i.e., $W > 24$ m, there is a decrease in the influence of the frontal inflow, while that of the corner-streams increases both at MS1E and MS2E, yielding *VR* of between 0.0903 and 0.1948 at MS1E and between 0.1189 and 0.2642 at MS2E. These values represent an increase of between 34% and 50% at MS1E and between 14% and 44% at MS2E. It would, thus, mean that the corner-stream has profound influence on the total inflow for this range of height ratio and separation distance, and that the relative influence of the frontal and the corner-stream inflows also depends on the dimension of the frontal opening, which in the current study is much smaller than that of lateral opening.

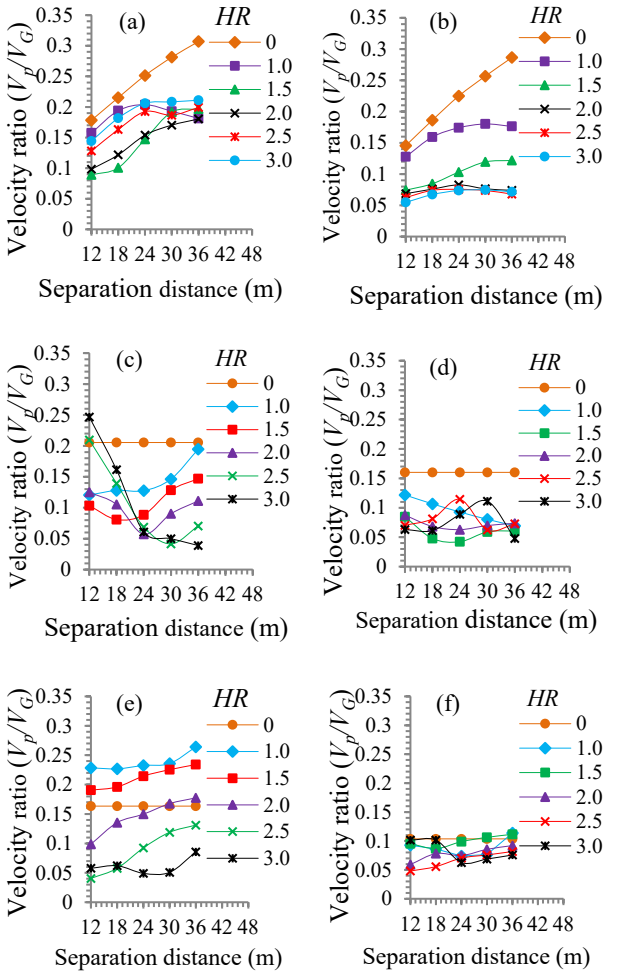

Fig. 10: *VR* profiles at various sections of the streets: (a) SSE, (b) SSM, (c) MS1E, (d) MS1M, (e) MS2E, (f) MS2M

As the height ratio increases, i.e., $HR > 2$, the reach of the frontal inflow and the length of throw of the corner-stream increase. For small separation distances therefore, the frontal inflow reaches fully into MS2E, but the corner-stream overshoots the side openings both at MS1E and MS2E. This yields *VR* of between 0.0608 and 0.2468 at MS1E, Fig.10(c), and between 0.0491 and 0.0924 at MS2E, Fig.10(e). When the separation distance increases, the fringes of the corner-stream inflow are just reaching MS1E, while the reach and impact of the frontal inflow at the street decreases. At MS2E, the frontal inflow is almost completely withdrawn but the corner-stream inflow is now being intercepted substantially into the street. For this range of *HR* and *W*, the *VR* is between 0.0389 and 0.0705 at MS1E and between 0.0509 and 0.1312 at MS2E. It would, therefore, mean that for buildings $HR>2.0$, *VR* around the downwind building array decreases with separation distance.

At the mid-street sections (Figs. 10(d) and (f)), the *VR* values are generally low at between 0.0478 and 0.1144 at MS1M, Fig.10(d), and between 0.0480 and 0.1063 at MS2M, Fig.10(f) for all *HR* and *W*, as the frontal inflows appear to be drawn more towards the sides and the corner-stream inflows do not extend to the streets. This may be due to size of the frontal opening which is small compared to that of the side openings.

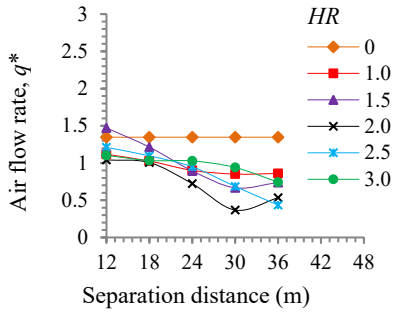

Fig. 11: Air flow rate characteristics for the objective domain

From Fig.11, it would be observed that around the downwind building array, the air flow rate *AFR* generally tends to decrease as the separation distance between the arrays increases, except for configurations $HR = 1$, 1.5 and 2 for which *AFR* begins to increase as from $W > 30$ m. The *AFR* decreases from a maximum in the range $1.1024 \leq AFR \leq 1.4704$ to some minimum values in the range $0.3674 \leq AFR \leq 0.4341$. This general trend is consistent with results indicated in Buccolieri et al.[12], and could indicate that less air flowrate at higher wind speed, indicated by the increasing velocity ratio for some configurations of the adjacent building arrays, may actually be occurring inside the street. However, the air flow rate does not appear to have a well-defined pattern of variation with height ratio. This may be due to the opposing influence the frontal and the corner-stream inflows have on the flow and ventilation around the downwind buildings.

Fig. 12 shows the characteristics of the air flow rate through the front (Fig.12(a)), rear Fig.12(b), sides (Fig.12(c), and top (Fig.12(d) openings of the objective domain. The figures are used to examine the level of contribution of each of the openings to the total air exchanges of the domain. It would be observed from the figure that compared to $HR > 0$ configuration, the reference configuration $HR = 0$ has the highest inflow through the frontal opening, except for configuration $HR = 1.5$, $W \leq 18$ m. Similarly, the outflow through the top opening is highest for the reference configuration. The air flow rate into the domain is least through the rear opening. No significant back flow is observed through any of the openings.

For $HR > 0$, it is indicated that the rate of air flow into the neighbourhood array through the frontal opening decreases as the separation distance increases, for all height ratios. However, the air flow rate increases as the height ratio increases. It may also be observed that the proportion of flow entering into the array is highest through the frontal opening (Fig.12(a)), while that through the rear opening is least, and which is through reverse flow for $HR > 1$ configuration (Fig.12(b)). For $HR = 1$ configuration, the outflow from the domain is through the

rear opening. The top opening serves as outflow for all the configurations, and for most of the configurations, has the highest rate of outflow (Fig.12(d)). The side openings admit about 50% of the total inflow into the array, particularly for $HR \leq 1.5$. However, for configuration $HR \geq 2$, the side opening also serves as the exit channel. For some configurations, the openings serve as the major exit channel, with the top openings providing only a fraction of the outflow, e.g., for $HR = 2.5$ and $HR = 3$ at $W = 12$ m, the side opening serves as the major exit channel, while the top opening provides only a fraction of the outflow (Figs. 12(c) and (d). It would also be observed from the figures that for all the configurations, the net inflow through the top opening is zero.

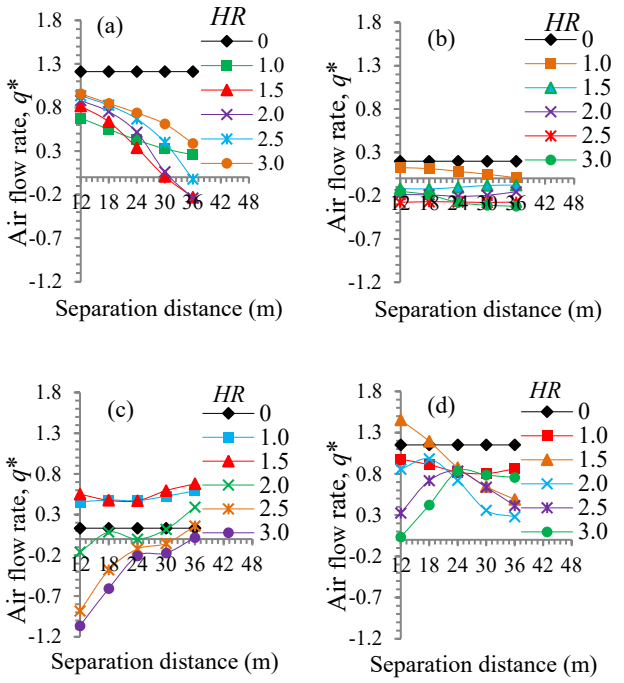

Fig. 12: Contributions of each boundary opening to overall air flow rate of the objective domain. (a) Front, (b) Rear, (c) Sides, (d) Top

To further investigate into the mechanism of flow that may be responsible for the characteristics of flow just observed, some typical flow patterns around the arrays of buildings were carefully examined. Fig. 13 shows such typical flow patterns at the pedestrian height for the half-domain of some configurations of the adjacent building arrays: $HR = 0$ (Fig.13(a)), $HR = 1$, $W = 12$ m (Fig.13(b)), $HR = 1$, $W = 36$ m (Fig.13(c)), $HR = 2$, $W = 12$ m (Fig.13(d)), $HR = 2$, $W = 36$ m (Fig.13(e)), $HR = 3$, $W = 12$ m (Fig.13(f)), and $HR = 3$, $W = 36$ m (Fig.13(g)). From the figure, it would be observed that there is a high-speed flow (indicated by the horizontal arrow in red colouration in Fig. 13(b)) that enters through the frontal opening into the domain of the adjacent buildings. It may also be seen that at $W = 12$ m, the high-speed inflow extends even into the objective domain. The extension of the frontal inflow increases with increase in height ratio. It can also be observed that at $HR = 1$, $W = 12$ m, the frontal inflow barely extends to MS1 (Fig.13(b)); at $HR = 2$, $W = 12$ m, it is fully into MS1 (Fig.13(d)), and at $HR = 3$, $W = 12$ m, the inflow reaches into MS2 (Fig.13(f)).

It may also be observed that the inflow tends to spread into the lateral streets to invigorate the flow in the streets, with SS being more affected at $HR = 1$ (Fig.13(b)), followed by MS1 that is only moderately affected at $HR = 2$ (Fig.13(d)), and then the same MS1 being more intensively affected at $HR = 3$ (Fig.13(f)). This could be as a result of the higher quantity of the approach flow that impinges on the windward face of the frontal rows of buildings as the height ratio increases. This gives rise to more flows being deflected down the face of the buildings and channeled through the frontal opening with increase in HR, extending further and further into the objective domain with the increase in HR.

It may also be observed from Fig.13 that with increase in the separation distance, there is a decrease in the reach of the frontal inflow, such that at $W = 36$ m the extension is almost limited to the SS, with the intensity of flow in the street increasing from when $HR = 1$ to $HR = 3$. This can be explained from the perspective that even though greater quantity of flow impinges on the faces of the frontal building as the height ratio increases, the increase in the separation distance has created room for expansion of the high-speed frontal inflow into SS, which is the easier path to take compared to having to force itself through the narrow frontal opening of the objective domain.

From Fig.13, it may be observed that there is a high-speed corner-stream flow that emerges from the far edge of the frontal buildings as indicated by the two curved arrows in red colouration. At $HR = 1$, a portion of the corner-stream tends to be flow into the side openings of the target domain, influencing the flow in MS1 and MS2, particularly at the edge sections, i.e., MS1E and MS2E. A greater proportion tends to overshoot the side openings. As the separation distance increases, more of the corner-stream flows into MS1 and MS2, with some portion even entering into SSE. This may be responsible for the increased velocity ratio that is observed in Fig.10 for these streets. Together with the influence of the frontal inflow at SS, the VR in the streets at HR=1 therefore tends to be high for all the streets.

As the height ratio increases and more quantity of the approach flow impinges on the wind ward faces of the frontal buildings, the quantity and intensity of the corner-stream increases. As a result, the quantity of the stream flowing into the lateral streets decreases, with the greater proportion overshooting the side openings. This behavior may be observed from Figs.13(b) – (g). The capability of the corner-stream to invigorate the flow in the lateral streets, thus, decreases with height ratio. This may be observed from VR characteristic behavior, (Fig.10).

From the foregoing, it would mean that there are two predominant sources through which the flow around the

adjacent building arrays is invigorated; they are the frontal inflow and the corner-stream flow. The frontal inflow tends to invigorate the flow within the separation street more that it does the other streets, while the corner-stream inflow tends to influence the flow around MS1 and MS2 more than it does the separation street. The influences of these flow sources tend not to be concurrent, particularly for the streets of the objective domain, i.e., they don't occur at the same time, except for *HR*=1. This means that at the time the frontal inflow is influencing the flow in the separation street, the corner-stream inflow is overshooting the side openings.

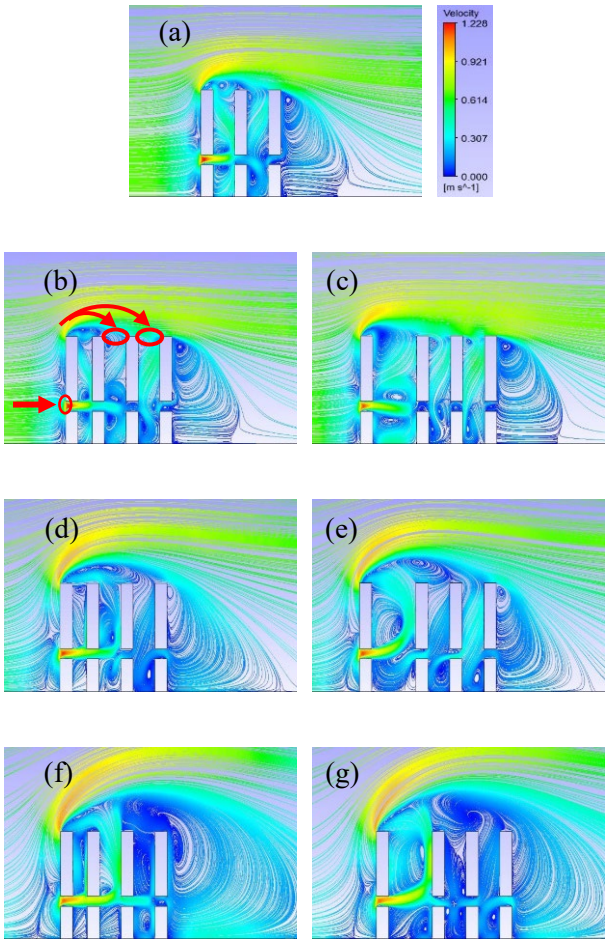

Fig. 13: Typical flow patterns at the pedestrian height for half-domain of the adjacent building arrays. (a) *HR* = 0, (b) *HR* = 1, *W* = 12 m, (c) *HR* = 1, *W* = 36 m, (d) *HR* = 2, *W* = 12 m, (e) *HR* = 2, *W* = 36 m, (f) *HR* = 3, *W* = 12 m, (g) *HR* = 3, *W* = 36 m

Small separation distances and small height ratios tend to make the influence of the frontal inflow more dominant than that of the corner-stream inflow, while larger separation distances increased the influence of the corner-stream inflow, as against that of the frontal inflow. Large height ratios also tend decrease the influence of the corner-stream, while increasing that of frontal inflow. It would thus, mean that for a particular configuration of the adjacent buildings, the separation distance that would enable optimum air flow and ventilation within the streets can be determined by carefully analyzing the flow for when the influences of these two flow sources best compliment themselves.

4. Conclusion

The effects of the interference to outdoor air flow and ventilation by a taller building array in an upwind location of another array of buildings of lower height have been examined by numerical simulation after initially validating the applicable turbulence model and ensuring that the model and settings for calculating the field of flow and, thus, predicting the ventilation performance around the building arrays were robust enough. The results demonstrated the mechanism of air flow and ventilation around the arrays of buildings and the effects on interference of locating a taller building array upwind of one with lower height. The effects of separation distance between the building arrays on two key thermal comfort indicators, i.e., air velocity ratio and air flow rate for different height ratios between the building arrays were also determined.

It is demonstrated in the study that two building arrays of dissimilar heights located in close proximity, with the taller array at the upwind location, can reduce the air velocity ratio and, thus, the speed of the wind at the pedestrian level height around the downwind array by as much as 80% at some of the street sections compared to when there is no interference effect at all. Separation distance can, however, be used to invigorate the flow by as much as 50% at some street sections of the downwind building array. The channel of flow of air into the downwind building array is predominantly through the frontal openings and the side openings; the flow speeds, indicated by air velocity ratio, through the openings, however, tend to be in inverse proportion to themselves. The frontal opening appears to be of little influence on the total inflow into the streets probably due to the size of the opening that is small compared to that of the lateral or side openings.

The air velocity ratio around the downwind buildings with and without a building array located at the upwind location are poorer at the interior streets. The presence of the upwind array of buildings reduces the *VR* around the streets of the downwind building array by as much as 61%. The *VR* does not appear to be influenced by separation distance. The air flow rate *AFR* generally tends to decrease as the separation distance. The trend is consistent with results of the study by Buccolieri et al.[12], and could indicate that less air flow rate at higher wind speed as obtainable in constricted flow may actually be occurring inside the street. The air flow rate does not appear to have a well-defined pattern of variation with height ratio.

The size of the frontal opening employed in this study is small in comparison to the size of the lateral opening and may be responsible for low inflow through the

opening. The next target of the study would, thus, be to examine the impact of size of the frontal opening on the air velocity ratio and the air flow rate. Also, the study has been limited to a maximum separation distance of 36 m and may be responsible for why the *VR* and *AFR* trend with separation distance has not been properly captured for *HR* > 2.0. It would therefore be necessary to investigate the flow around the adjacent building arrays for greater separation distances and large height ratios.

The findings of this study could be applied in the building industry by building professionals and relevant government agencies for appropriately laying out residential building arrays for enhanced performance of the flow and air ventilation around the buildings, particularly in low-wind climatic environments.

Acknowledgements

We wish to express our sincere gratitude to the Centre for Information and Communication Technology (CICT) Unit and the management of Universiti Teknologi Malaysia (UTM) for providing the High Performance Computing (HPC) facility with which the CFD numerical simulation was implemented.

Nomenclature

AFR	Air flow rate (-)
B	Universal constant (-)
COST	European Cooperative in the Field of Scientific and Technical Research
C_S	Surface roughness constant (-)
C_μ	Model constant of the Standard *k*-*ε* model (-)
D	Building depth (m)
H	Building height (m)
HR	Height ratio (-)
k	Turbulence kinetic energy per unit mass (m^2/s^2)
k_p	Turbulence kinetic energy at centre-point of near wall cell (m^2/s^2)
K_S	Dimensional roughness height (-)
K_S^+	Dimensionless surface roughness height (-)
MS	Main street
MS1	Main street 1
MS1E	Main street 1 edge
MS1M	Main street 1 middle
MS2	Main street 2
MS2E	Main street 2 edge
MS2M	Main street 2 middle
$\vec{n}$	Unit vector normal to the surface of an opening (-)
q	Flow rate (m^3/s)
q^*	Normalized flow rate (-)
RKE	Realizable turbulence kinetic energy
SS	Separation street
SSE	Separation street edge
SSM	Separation street middle
U	Horizontal velocity, characteristic velocity of mean flow, mean velocity (m/s)
U_p	Horizontal component of wind velocity at center-point of near wall cell (m/s)
u^*	Friction velocity for constant flux boundary layer (m/s)
Udf	User defined function
V	Velocity, mean velocity component in the *y*-direction (m/s)
$\vec{V}$	Velocity vector (m/s)
VR	Air velocity ratio (-)
w	Lateral passage between buildings (m)
W	Width of building, longitudinal separation distance between frontal building column and objective domain (m)
W_c	Constant longitudinal passage width between buildings of objective domain (m)
x	Longitudinal Cartesian coordinate (m)
y	Vertical Cartesian coordinate (m)
y_0	Aerodynamic roughness height (m)
y_p	Distance between centre-point *P* and wall (m)
z	Lateral Cartesian coordinate (m)

Greek symbols

ε	Dissipation rate of turbulence kinetic energy (m^2/s^3)
ε_p	*ε* at the center-point of near wall cell (m^2/s^3)
κ	von Karman constant (-)
ν	Kinematic molecular viscosity of fluid (m^2/s)

Subscripts

c	Constant
0	Aerostatic reference, reference state
p	Center-point of near wall cell
s	Surface
μ	Dynamic molecular viscosity of fluid

References

1) S.H.L. Yim, J.C.H. Fung, A.K.H. Lau, and S.C. Kot, "Air Ventilation Impacts of the 'Wall Effect' Resulting from the Alignment of High-Rise Buildings," *Atmospheric Environment*, 43 (*32*) 4982-4994 (2009). doi:10.1016/j.atmosenv.2009.07.002.
2) W. Ji, B. Zhao, "Numerical study of the effects of trees on outdoor particle concentration distributions,"

Building Simulation, 7 417-427 (2014).

2) W. Ji, B. Zhao, "Numerical study of the effects of trees on outdoor particle concentration distributions," *Building Simulation*, 7 417-427 (2014).
3) A.F. Mohammed, N. kegaya, R. Hikizu, S.H. Zaki, "Turbulence Effect of Urban-Canopy Flow on Indoor Velocity Fields under Sheltered and Cross-Ventilation Conditions," *Sustainability*, 13 (*586*) 1-11 (2021). doi:10.3390/su13020586.
4) A. Leelossy, F.M. Jr, F. Izsak, A. Havasi, I. Lagzi, R. Meszarou, "Dispersion modeling of air pollutants in the atmosphere: a review," *Central European Journal of Geosciences*, 6 (*3*) 257-278 (2014). doi:10.2478/s13533-012-0188-6.
5) Namrata, N.D. Wagh, "A Review on Atmospheric Dispersion System for Air Pollutants Integrated with GIS in Urban Environment," *Nature Environment and Pollution Technology: An International Quarterly Scientific Journal*, 21 (*4*) 1553-1563 (2022). doi:10.46488/NEPT.2022.v21i04.008.
6) S.A. Zaki, N.F.M. Kasim, N. Ikegaya, A. Hagishima, M.S.M. Ali, "Numerical Simulation on Wind-Driven Cross Ventilation in Square Arrays of Urban Buildings with Different Opening Positions," *Journal of Advanced Research in Fluid Mechanics and Thermal Sciences*, 49 (*2*) 101-114 (2018). ISSN: 2289-7879.
7) S.A. Zaki, A. Hagishima, J. Tanimoto, "Experimental study of wind-induced ventilation in urban building of cube arrays with various layouts," *Journal of Wind Engineering and Industrial Aerodynamics*, 103 31-40 (2012). doi:10.1016/j.jweia.2012.02.008.
8) H. Tan, K.Y. Wong, C.T. Lee, S.L. Wong, B.B. Nyakuma, R.A. Wahab, K.Q. L, M.C. Chiong, W.S. Ho, M.H.D. Othman, Y.H. Yau, H.Y. Kek, H.M. Kamar, "Numerical assessment of ceiling-mounted air curtain on the particle distribution in surgical zone," *Journal of Thermal Analysis and Calorimetry*, 148 3005-3018 (2023). doi:10.1007/s10973-022-11466-6.
9) P. Byrne, N. Putra, T. Mare, N. Abdullah, P. Lalanne, I. Alhamid, P. Estelle, A. Yatim, and A-L. Tiffohhet, "Design of solar AC system including a PCM storage for sustainable resorts in tropical region," *Evergreen*, 6 (*2*) 143-148 (2019). doi:10.5109/2321009.
10) Y-D. Kim, K. Thu, and K.C. Ng, "Evaluation and parametric optimization of the thermal performance and cost effectiveness of active-indirect solar hot water plants," *Evergreen*, 2 (*2*) 50-60 (2015). doi:10.5109/1544080.
11) Y.T. Arbirham, K. Thu, T. Miyazaki, and N. Takata, "Comparative study of thermal water pumping cycles," *Evergreen*, 8 (*1*) 239-248 (2021). doi:10.5109/4372284.
12) R. Buccolieri, M. Sandberg, and S. Di Sabatino, "City Breathability and its Link to Pollutant Concentration Distribution within Urban-like Geometries," *Atmospheric Environment*., 44 (*15*) 1894-1903 (2010). doi:10.1016/j.atmosenv.2010.02.022.
13) L. Chen, J. Hang, M. Sandberg, L. Claesson, and S. Di Sabatino, "The Influence of Building Packing Densities on Flow Adjustment and City Breathability in Urban-like Geometries," *Procedia Engineering*., 98, 758–769 (2017). doi:10.1016/j.proeng.2017.12.127.
14) F. Yang, Y. Gao, K. Zhong, and Y. Khang, "Impacts of Cross-Ventilation on the Air Quality in Street Canyons with Different Building Arrangements," *Building and Environment*., 104 1-12 (2016). doi:10.1016/j.bildenv.2016.12.04.013.
15) W. You, J. Shen, and W. Ding, "Improving Residential Building Arrangement Design by Assessing Outdoor Ventilation Efficiency in Different Regional Spaces," *Architectural Science Review*., (2018). doi: 10.1080/00038628.2018.1471388.
16) T. van Hooff, and B. Blocken, "On the effect of wind direction and urban surroundings on natural ventilation of a large semi-enclosed stadium," *Computers and Fluids*., 39 1146–1155 (2010). doi:10.1016/j.compfluid.2010.20.004.
17) J.S. Park, "Long-term field measurement on effects of wind speed and directional fluctuation on wind-driven cross ventilation in a mock-up building," *Building and Environment*., 62 1–8 (2013). doi:10.1016/j.buildenv.2012.12.013.
18) R. Buccolieri, P. Salizzoni, L. Soulhac, V. Garbero, and S. Di Sabatino, "The Breathability of Compact Cities," *Urban Climate*., 13 73–93 (2015). doi:10.1016/j.uclim.2015.06.002.
19) H. Gough, T. Sato, C. Halios, C.S.B. Grimmond, Z. Luo, J.F. Barlow, A. Robertson, R. Hoxey, and A. Quinn, "Effects of variability of local winds on cross ventilation for a simplified building within a full-scale asymmetric array: Overview of the Silsoe field campaign," *Journal of Wind Engineering & Industrial Aerodynamics*., 175 408-418 (2018). doi:10.1016/j.jweia.2018.02.010.
20) H. Han, M. Hatta, and H. Rahman, "Smart ventilation for energy conservation in buildings," *Evergreen*, 6 (*1*) 44-51 (2019). doi:10.5109/2321005.
21) D.A. Wulandari, M. Akmal, Y. Gunawan, and Nasruddin, "Cooling improvement of the IT rack by layout arrangement of the A2 Class Data Centre Room: A simulation study," *Evergreen*, 7 (*4*) 489-499 (2020). doi:10.5109/4150468.
22) W.K. Yinn, H.M. Kamar, N. Kamsah, and A.S. Norazam, "Effects of surgical staff turning motion on airflow distribution inside a hospital operating room," *Evergreen*, 6 (*1*) 52-58 (2019). doi:10.5109/2321008.
23) A.D. Pendwarden, and A.F.E. Wise, "Wind Environment around Buildings,". Building Research Establishment Report. Department of Environment, BRE, Her Majesty's Stationery Office, London, UK, 1975. https://g.co/kgs/myadwu.
24) H.L. Khalid, and A.M.A Rahman, "Harvesting wind

power from air-conditioning exhaust air as an alternative way in optimizing wind power in tropical Malaysia," *Proc. of the 5th IBC, Kyoto, Japan, May 28-31*, 1331-1338 (2012). https://www.researchgate.net/publication/326649105.

25) M.H. Hanipah, A.H. Abdullah, N.A.C. Sidik, R. Yunus, M.N.A.Yasin, and M.N.A.W.M. Yazid, "Assessment of outdoor thermal comfort and wind characteristics at three different locations in Peninsular Malaysia," *Proc. MATEB Web of Conferences*, 47 (*04005*) (2016). doi:10.1051/matecconf/20164704005.
26) T.W. Wen, C. Palanichamy, and G. Ramasamy, "Performance optimization of constant speed – small horizontal axis wind turbine for wind energy development in Malaysia," *International Journal of Energy Economics and Policy*, 9 (*3*) 280-290 (2019). doi:10.32479/ijeep.7567.
27) S.A. Ayo, N.M. Ghazali, and S. Mansor, "Outdoor ventilation performance of various configurations of a layout of two adjacent buildings under isothermal conditions," *Building Simulation*, 8 (*1*) 81-98 (2015). doi:10.1007/s12273-014-0195-2.
28) A.M. Nugroho, M.H. Ahmad, and D.R. Ossen, "A Preliminary study of thermal comfort in Malaysia′s single-storey terrace houses," *Journal of Asian Architecture and Building Engineering*, 6 (*1*) 175-182 (2007). doi:10.3130/jaabe.6.175.
29) Malaysia Uniform Building By-Laws 1984 (UBBL) 2006 Amendment, MDC Publishers, Kuala Lumpur (2006).
30) Malaysia Planning Guideline (GP022) - *Gated community and guarded neighbourhood (GP022)*, First ed. Malaysia: Federal Town and Country Planning Department Peninsular Malaysia, Ministry of Housing and Local Government (2010).
31) T.H. Shih, W.W. Liou, A. Shabbir, Z.Yang, and J. Zhu, "A New *k–ε* Eddy Viscosity Model for High Reynolds Number Turbulent Flows,". *Computers & Fluids*, 24 227–238 (1995). doi:10.1016/0045-7930(94)00032-T.
32) H. Montazeri, B. Blocken, "CFD simulation of wind-induced pressure coefficients on buildings with and without balconies: Validation and sensitivity analysis," *Building and Environment*, 60 137-149. (2013).
33) W. Janssen, B. Blocken, T. van Hooff, "Pedestrian wind comfort around buildings: Comparison of wind comfort criteria based on whole-flow field data for a complex case study," *Building and Environment*, 59 547–562 (2013).
34) B. Blocken, "LES over RANS in building simulation for outdoor and indoor applications: A foregone conclusion?," *BUILDING SIMULATION*, 11 821–870 (2018). doi.10.1007/s12273-018-0459-3.
35) W.A. Hoydysh, "Scale Model Study of Dispersion of Pollutant in Street Canyons. *In: 67th Annual Meeting of the Air Pollution Control Association (APCA)*, Denver, CO, 74–157 (1974).
36) J. Franke, A. Hellsten, K.H. Schlunzen, B. Carissimo, and editors, "*Best practice guideline for the CFD simulation of flows in the urban environment. COST Action 732, quality assurance and improvement of microscale meteorological models*," Brussels, COST office, (2007). https://www.researchgate.net/publication/25776/2093.
37) Y. Tominaga, A. Mochida, R. Yoshie, H. Kataoka, T. Nozu, M. Yoshikawa, and T. Shirasawa, "AIJ Guidelines for Practical Applications of CFD to Pedestrian Wind Environment around Buildings," *Journal of Wind Engineering and Industrial Aerodynamics*, 96 (*10*) 1749-1761 (2008). doi:10.1016/j.jweia.2008.02.058.
38) P.J. Richards, and R.P. Hoxey, "Appropriate boundary conditions for computational wind engineering models using the k-ϵ turbulence model," *Journal of wind engineering and industrial aerodynamics*, 1993 (*46*) 145-153 (1913). doi:10.1016/B978-0-444-81688-7.50018-8.
39) ANSYS Fluent 14.0, "*User's Guide*," ANSYS Inc., Canonsburg, PA, (2011). https://www.pdfdrive.com/ansys-fluent--140-users-guide-e188401578.html.
40) V.T. Tran, Y.H.P. Duong, T.M. Le, "The Influence of Meshing Strategies on The Numerical Simulation of Solar Greenhouse Dryer," *IOP Conference Series: Earth and Environment Science*, 947 012007 (2021). doi:10.1088/1755-1315/947/1/012007.
41) J. Franke, C. Hirsch, A.G. Jensen, H.W. Kru¨ s, M. Schatzmann, P.S. Westbury, S.D. Miles, J.A. Wisse, and N.G. Wright, "Recommendations on the use of CFD in wind engineering,". *Proceedings of the In: Proceedings of the International Conference on Urban Wind Engineering and Building Aerodynamics. In: van Beeck, J.P.A.J.(Ed.), COST Action C14, Impact of Wind and Storm on City Life Built Environment*, 5–7 May (2004). https://www.researchgate.net/publication/251814717
42) I. Džijan, Z. Virag, S. Krizmanić, "Comparison Of The Simpler And The Simple Algorithm For Solving Navier-Stokes Equations On Collocated Grid," *Transactions of FAMENA*, (2006). ISSN 1333-1124
43) B. Blocken, T. Stathopoulos, J. Carmeliet, "Wind environmental conditions in passages between two long narrow perpendicular buildings," *Journal of Aerospace Engineering*, 21 (4) 280-287 (2008).
44) J. Wieringa, "Updating the Davenport Roughness Classification," *Journal of Wind Engineering and Industrial Aerodynamics*, 41 (*1*) 357-368 (1992). doi:10.1016/0167-6105(92)90434-C.
45) E. Ng, L. Katzschner, U. Wang, C. Ren, and L. Chen, "*Working Paper No. 1A: draft urban climatic analysis map–urban climatic map and standards for*

wind environment–feasibility study," Technical Report for Planning Department HKSAR. Report No. WP1A, Planning Department of Hong Kong Government: Hong Kong, (2008). https://www.pland.gov.hk/pland_en/p_study/prog_s/ucmapweb/ucmap_project/content/reports/wp1a.pdf.

46) K. Uehara, S, Murakami, S. Oikawa, and S. Wakamatsu, "Wind Tunnel Experiments on How Thermal Stratification Affects Flow in and above Urban Street Canyons," *Atmospheric Environment*, 34 (*10*) 1553-1562 (2000). doi:10.1016/51352-2310(99)00410-0.

47) X. Xie, C.-H. Liu, and D.Y.C. Leung, "Impact of Building Facades and Ground Heating on Wind Flow and Pollutant Transport in Street Canyons," *Atmospheric Environment*, 41 (*39*) 9030-9049 (2007). doi:10.1016/j.atmosenv.2007.08.027.

48) R. Yoshie, A. Mochida, Y. Tominaga, H. Kataoka, K. Harimoto, T. Nozu, and T. Shirasawa, "Cooperative Project for CFD Prediction of Pedestrian Wind Environment in the Architectural Institute of Japan," *Journal of Wind Engineering and Industrial Aerodynamics*, 95 1551–1578 (2007). doi:10.1016/j.jweia.2007.02.023.

49) J.O.P. Cheung, and C.-H. Liu, "CFD simulations of natural ventilation behaviour in high-rise buildings in regular and staggered arrangements at various spacings," *Energy and Buildings*, 43 1149–1158 (2011). doi:10.1016/j.enbuild.2010.11.024.

50) T.S. Boutet, "*Controlling Air Movement: A Manual for Architects and Builders"*: McGraw-Hill, (1987). https://www.amazon.com/controlling-air-movement-architects-builders/dp/0070067139.

51) B. Blocken, and J. Carmeliet, "Pedestrian Wind Environment around Buildings: Literature Review and Practical Examples," *Journal of Thermal Envelope and Building Science*, 28 (*2*) 107-159 (2004). doi:10.1177/1097196304044396.